journal

J. Am. Ceram. Soc., 72 [7] 1192-99 (1989)

Binder Distribution in Ceramic Greenware During Thermolysis

Michael J. Cima,* Jennifer Alan Lewis,* and Alan D. Devoe

Ceramics Processing Research Laboratory, Materials Processing Center, Massachusetts Institute of Technology, Cambridge, Massachusetts 02139

Capillary forces were shown to influence the distribution of polymer–plasicizer mixtures within ceramic green bodies during binder thermolysis. Isothermal thermogravimetric analysis was performed on tape-cast sheets of an alumina–poly(vinyl butyral)–dibutyl phthalate composite and direct observations were made of the binder distribution and pore growth after partial pyrolysis. This led to the investigation of a model system, an alumina–eicosane composite, by similar experimental techniques. The early stage of binder removal was found to be similar to the drying of particle beds in which capillary forces draw liquid into the smaller pores at the surface. The morphology of the binder distribution produced by these processes dictates which mass-transfer resistances may be controlling in binder burnout. A model is described that determines the length scale over which capillarity acts based on measurable physical parameters of the binder system and the packing of the ceramic particles. [Key words: binders, green bodies, thermal analysis, modeling, capillarity.]

I. Introduction

BINDER is most frequently removed by thermal decomposition of the polymeric binder. In this process high production rates of volatile species must be avoided, and those volatile species that are produced must be allowed to diffuse to the surface of the ceramic piece without forming defects within the green body. The important issues in binder removal fall naturally into two categories: chemical and physical. The chemical aspect of binder removal pertains to the rate at which volatile products are produced and to the process design that minimizes residual carbon in the ceramic green body. The physical aspect involves the relationship between binder removal and mass- and heat-transfer limitations, as well as changes in particle packing.

Little is known about the changes in binder distribution that occur during burnout and how these changes influence stress within the green body, and the magnitude of the mass- and heat-transfer resistances present in the green body have not yet been evaluated. These parameters are critical for the design of efficient heating schedules to prevent the formation of defects in many ceramic devices.

The issues of mass/heat transport, chemical kinetics, and binder distribution are intimately coupled in the binder-burnout process. The rate at which volatile products are generated is primarily determined by the rate at which heat is applied to the greenware. The binder distribution determines the path length over which volatile products must diffuse or migrate, and the pore structure determines the mass-transfer resistance opposing the transport of these species. In a mathematical sense, the binder distribution and shape of the greenware describe the boundary conditions under which the differential equations for transport operate. The ability to predict both the rate at which binder is removed for a given set of conditions and the demands that the removal process makes on the structure of the part would allow improved design of ceramic parts and binders, minimizing or eliminating defects. However, this requires an adequate understanding of the above parameters.

A pedestrian view of the binder-burnout process is illustrated in Fig. 1. Heat is supplied to the surface of the green body to provide both the latent heat of vaporization of volatile products and the heat required for endothermic degradation of the polymeric binder. Volatile products are produced throughout the body and must diffuse to the surface. The material near the surface of the body can be removed faster than that near the center because of the shorter diffusion distance. In this simple picture, then, a region completely devoid of binder progressively grows toward the center of the body. Because of the difference in diffusivities in liquid and vapor phases, the model suggests that the controlling mass-transfer resistance would be in the liquid phase for most of the burnout process because the diffusion distances for liquid and vapor diffusion are of the same order. It will be shown that this simple model has two principal shortcomings: It neglects the fact that many binder systems are composed of materials that differ greatly in volatility and that transport of material in porous bodies can occur by mechanisms other than diffusion.

This paper describes observations of physical phenomena occurring during binder removal from alumina green tape. Two binder systems were investigated. System No. 1 consisted of a polymeric binder, poly(vinyl butyral) (PVB), and a plasticizer, dibutyl phthalate (DBP). Similar multicomponent binder systems have been discussed in the open literature.[1] System No. 2 consisted of pure eicosane, a 20-carbon alkane, that melts at 37°C and boils at 343°C. Eicosane–alumina composites were chosen as a model system because eicosane is available in pure form and has a vapor pressure that is high enough to allow removal without chemical degradation, which would complicate our interpretation of the physical aspects of binder thermolysis. In addition, the viscosity of eicosane, although lower than that of the PVB–DBP mixture, is high enough to prevent slumping of the cast sheet. It is proposed that binder is removed from these systems by transport phenomena similar to those found in the drying of solvents from particle beds and that this has important implications for describing the transport mechansims that govern binder burnout.

II. Experimental Procedure

A major issue that is common to most studies in ceramics processing is the reproducible fabrication of green microstructures on a laboratory scale. This difficulty was overcome for the alumina–PVB composites by obtaining industrially fabricated alumina/binder green sheets produced by tape casting. All the samples used in this study were made from a single lot of this tape, which contained 17 wt% binder consisting of two parts PVB* and one part DBP. The tape was very uniform in thickness (0.28 mm (0.011 in.)) and could easily be cut into samples 0.5 cm × 1 cm.

Alumina–eicosane composite sheets were formed by the following procedure. First, the appropriate amount of eicosane, cor-

S. C. Danforth — contributing editor

Manuscript No. 199165. Received May 3, 1988; approved November 23, 1988.
Supported by the MIT–Industry Ceramics Processing Research Laboratory Consortium.
*Member, American Ceramic Society.
*B-79, Monsanto, St. Louis, MO.

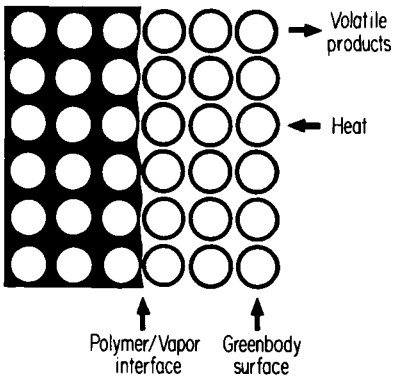

Fig. 1. Schematic of a simplified model of the binder-burnout process.

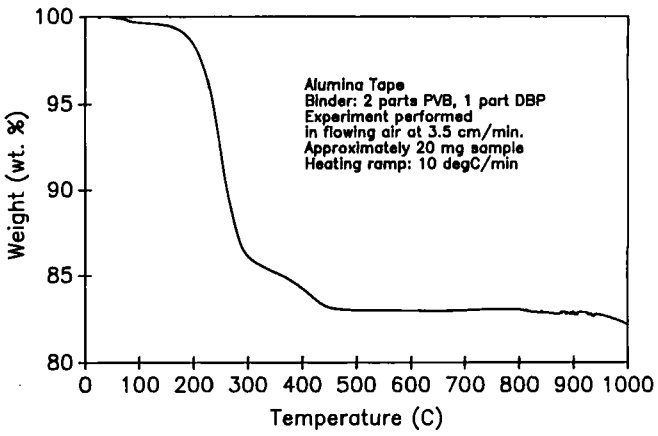

Fig. 2. Thermal gravimetric analysis of Al_2O_3–PVB–DBP tape.

responding to 15% by weight of alumina, was melted in a glass beaker. Oleic acid was then added (3% by weight of alumina) to the molten eicosane as a dispersant for the alumina. Finally, 20 g of alumina powder was added. After the temperature of the slurry equilibrated, the slurry was stirred and then cast. The casting procedure consisted of placing a few grams of the slurry on a Mylar-coated[†] glass plate and then pressing down on the deposited slurry with another Mylar-coated glass plate until the desired thickness was reached. The thickness of the cast tape ranged from 0.0041 to 0.0056 mm (0.016 to 0.022 in.), and samples 0.5 cm × 1 cm were easily cut. Examination of the cross section of the green tape by scanning electron microscopy (SEM) showed a fairly homogeneous microstructure with no apparent macrodefects.

Samples could be burned out to different extents by monitoring the mass by thermal gravimetric analysis (TGA)[‡] and quenching the experiment at the desired weight. Experiments for the PVB–alumina tape were performed in both air and argon with no apparent differences in behavior over the temperature range studied, whereas the eicosane composite was exposed to argon only (60 ppm of oxygen). During operation, the furnace was flushed continuously with gas so that the gas velocity was maintained at 3.5 cm/min. Both constant-heating-rate and isothermal experiments were performed in the same apparatus. Because of the lower viscosity of the eicosane, the eicosane–alumina composites had to be placed flat on a small piece of aluminum foil within the TGA pan, whereas the PVB composites could be leaned against the side of the pan with only small distortions developing during heat treatment. The eicosane–alumina samples did, however, maintain their shape as they were heat-treated and showed no tendency to spread in the bottom of the sample pan.

The pores of the partially burned-out tapes were stained so that they could be resolved when a fracture surface of a cross section of each tape was observed in an optical microscope. The stain consisted of a saturated potassium permanganate solution with several drops of detergent to lower the surface tension of the liquid. Samples were soaked for 1 min, allowed to dry for 0.5 h, then soaked for another minute. The fracture was initiated with a razor blade by scoring one edge of the tape. The orientation of each tape was carefully noted throughout the tests to examine whether differences existed in the way the bottom or the top burned out.

A mercury porosimeter[§] was used to measure the bulk density of the partially burned-out tape, as well as the pore volume and incremental intrusion. The porosimeter required larger samples than could be obtained from the TGA apparatus; therefore, larger sections of tape were cut and partially burned out in a small box furnace with a programmable temperature controller. The amount of binder removed was determined by measuring the mass of the sample before and after heat treatment.

III. Results and Discussion

As shown in the TGA trace in Fig. 2, the decomposition behavior of the binder mixture was very much like that found for pure PVB, where degradation occurs rapidly at temperatures above 200°C to produce a small amount of material that decomposes slowly between 300° and 400°C. The optical micrographs in Fig. 3 show the penetration of the potassium permanganate stain in progressively burned-out tapes. Although the stained region does appear to proceed as a front into the tape as the binder was removed, the model depicted in Fig. 1 cannot adequately account for the fact that stain can be observed throughout the tape when as little as 35% of the binder was removed. The penetration depth was found to be largely the same for the top and bottom of the tape (Fig. 4). Clearly, the presence of connected pores throughout the tape when 35% of the binder was removed is associated with the removal of plasticizer in the initial green tape.

Mercury porosimetry experiments were performed on partially burned-out tapes in order to characterize the developing porosity. The incremental-intrusion (V/D) curves shown in Fig. 5 reveal systematic trends in the porosity as the binder was removed. One can observe, for instance, that the area under each curve increases with increasing burnout. This is expected since this area represents the total volume intruded. This volume was found to increase linearly with increasing organic removal (Fig. 6). Also evident from the incremental-intrusion volume is an apparent trend to smaller values of the percolative-intrusion pore size as the binder was removed.

The percolative-intrusion size of the pores is that pore diameter calculated from the pressure measured when the incremental-intrusion volume is at a maximum. This quantity has been shown to be fundamentally different from the average or most frequent pore size since it is based on the intrusion of mercury from the surface of the sample.[2] This type of measurement tends to underestimate the volume of larger pores and overestimate that of smaller pores. Thus, the breadth of incremental-intrusion curves gives a highly distorted distribution in pore sizes. Nonetheless, the percolative-intrusion size does characterize the dimensions of pores, especially when comparing similarly prepared samples. Figure 7 shows that there was a 15% reduction in the characteristic size of the pores as binder was removed. This decrease in pore size cannot be explained by shrinkage of the tape since the tape density indicates that there was less than 1% linear shrinkage during burnout (Fig. 8).

The segregation of the binder to the smaller pores during burnout can be explained by binder movement under the influence of

[†]E. I. du Pont de Nemours & Co., Wilmington, DE.
[‡]Model TAS 7, thermal analysis system, Perkin-Elmer, Hartford, CT.
[§]Micromeritics Instrument Corp., Norcross, GA.

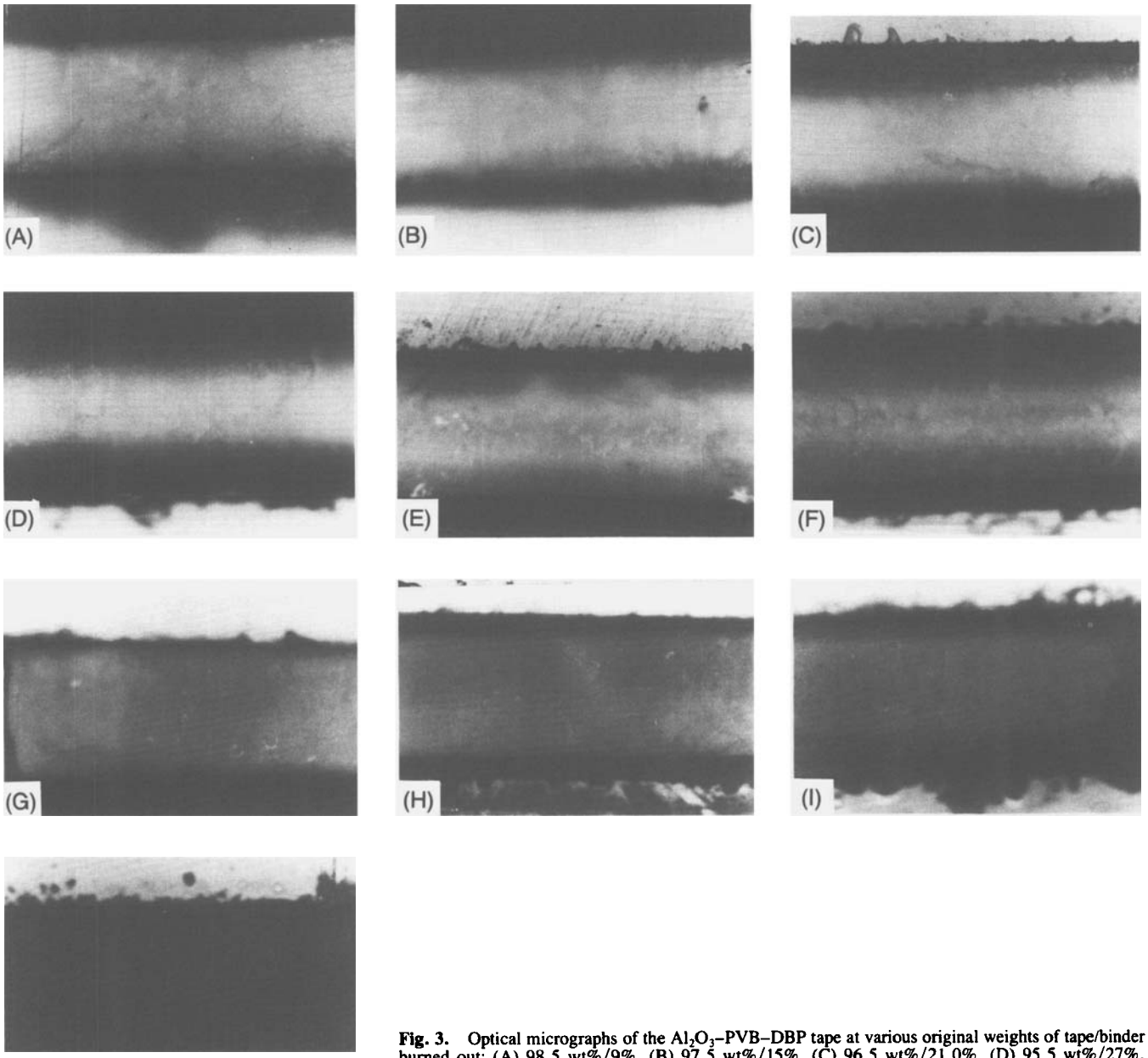

Fig. 3. Optical micrographs of the Al_2O_3–PVB–DBP tape at various original weights of tape/binder burned out: (A) 98.5 wt%/9%, (B) 97.5 wt%/15%, (C) 96.5 wt%/21.0%, (D) 95.5 wt%/27%, (E) 94.3 wt%/34.5%, (F) 93 wt%/42%, (G) 92 wt%/48.5%, (H) 90.5 wt%/58%, (I) 89.5 wt%/63.5%, and (J) 86 wt%/85%.

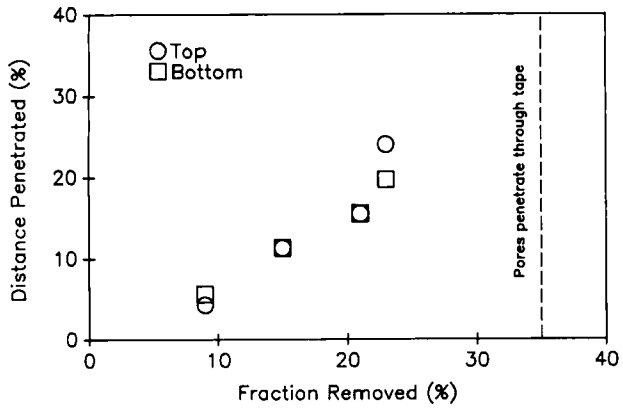

Fig. 4. Penetration of the stain into tape as binder is removed.

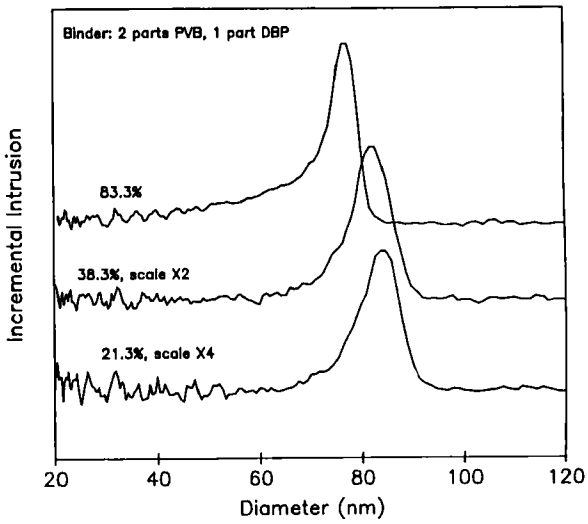

Fig. 5. Incremental intrusion versus pore size for partially dewaxed tapes.

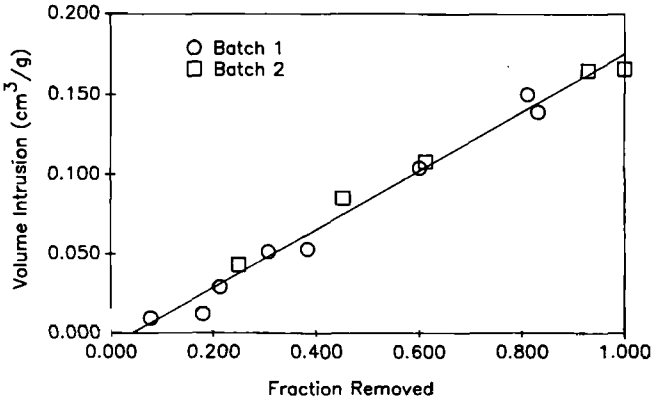

Fig. 6. Percolative volume versus fraction of binder removed.

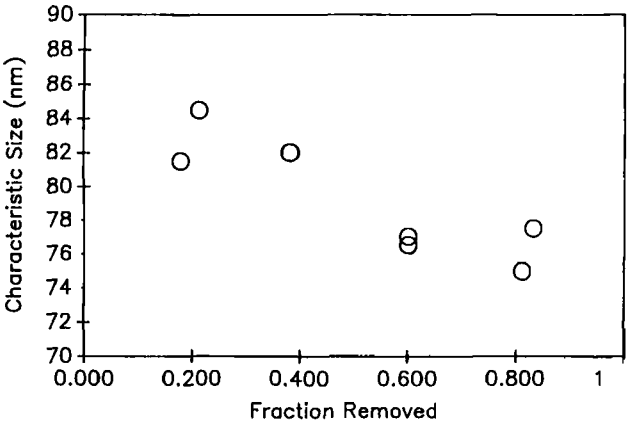

Fig. 7. Characteristic size of pores versus fraction of the binder removed.

capillary forces. Such a mechanism is analogous to that occurring during the drying of solvents from porous bodies. The internal distribution of liquids in porous beds during drying has been the subject of numerous investigations.[3] Most of the early work centered on the question of whether the mass transfer occurred by diffusion processes or by a different mechanism. Comings and Sherwood[4] and Ceaglske and Hougen[5] clearly showed that liquid motion occurs through the action of local variations in pore suction pressure due to variations in particle packing. Liquid–vapor meniscuses in smaller pores where local particle packing is high produce a larger suction pressure than do meniscuses in pores where the particle packing is not as dense. This relationship is described by the well-known equation of Young and Laplace:

$$P_s = \frac{2\gamma}{r} \tag{1}$$

where P_s is the suction pressure of a pore of radius r, containing a liquid–vapor interface with a surface tension γ.

The microscopic distribution of liquids within porous bodies was described by Shaw.[6] Although this model is based on equilibrium arguments, it has important implications for the dynamic case considered here. Minimization of the free energy requires that, above a critical volume fraction, the liquid must distribute to fill the smallest pores present in the body rather than distributing homogeneously throughout the porous structure at the necks of particle–particle contact. Thus, it is clear that there is a local thermodynamic driving force for fluid to segregate to the smallest pores.

Liquid in an initially saturated porous body continues to evaporate from the surface of the body as it dries since the smallest of the pores at the surface are continually supplied with liquid from the larger pores deep within the porous body because of the hydrostatic pressure difference created by the difference in suction pressures. This situation is depicted in Fig. 9. Liquid thus remains at the surface during a significant portion of the drying process.

This constant resupply of the surface permits the establishment of a steady state, or "constant-rate drying," which would not be possible if the liquid–vapor interface retreated into the body as it dried. The latter case would produce an increasing diffusion distance for the vapor component to overcome; thus the drying rate would continuously fall and a steady state would not be possible. Capillarity dictates that, in the case of drying, mass-transfer control is relegated to the boundary layer between the surface of the body and the free gaseous environment. This state is maintained until liquid cannot be supplied at a sufficient rate to keep the surface wet.

Figures 10 and 11 show the results of a series of isothermal experiments at different temperatures. After an initial transient as the samples came to a thermal steady state, constant rates are clearly observed at temperatures lower than 170°C, followed after some time by a falling rate period. The steady-state rate of removal of volatile products increased as the temperature increased because of the rising vapor pressure of the plasticizer.

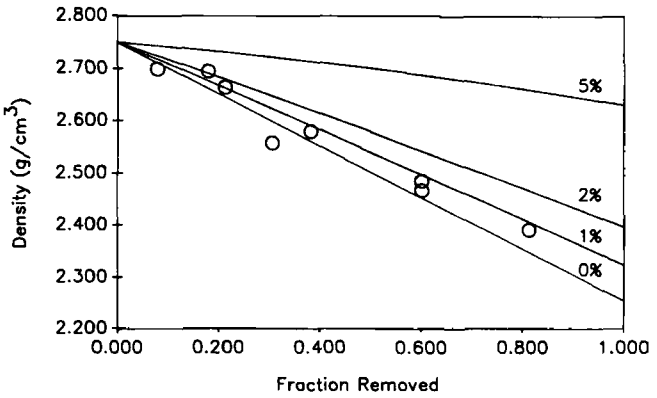

Fig. 8. Density of tape versus fraction of binder removed. Lines depict the calculated behavior of different linear-shrinkage values.

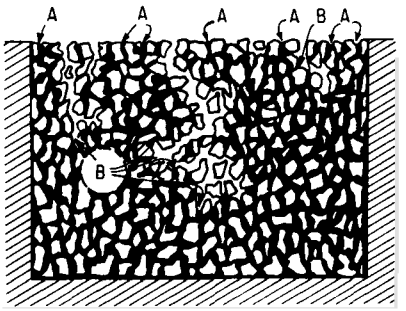

Fig. 9. Schematic of the motion of liquid due to capillary forces, similar to an illustration in Ref. 4. Small pores at points like *A* draw liquid from larger pores *B* as vapor leaves the surface of the porous body.

The amount of material removed during the constant-rate period was similar to the amount of plasticizer but decreased as the temperature increased. As volatile products are removed, the distance over which liquid must be drawn to the surface increases. The viscous resistance to flow through the green body increases as this distance increases and as the rate at which liquid must flow increases. At high mass-removal rates and for larger parts, a transition must occur where liquid for a given capillary force cannot be supplied fast enough. This transition marks the change from mass-transfer control outside the green body to a controlling mechanism within it.

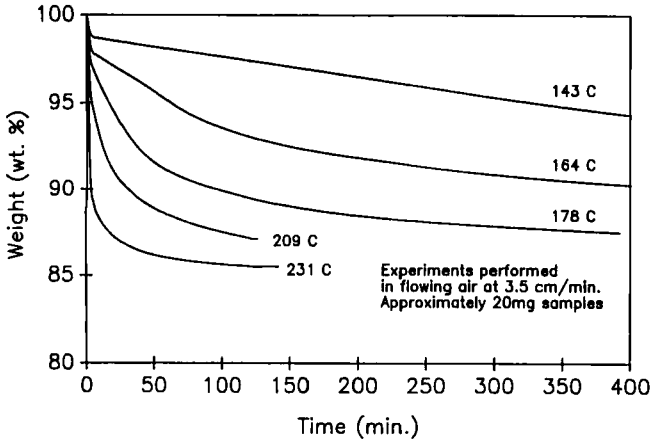

Fig. 10. Isothermal TGA indicating periods of constant rate of binder removal at temperatures lower than 170°C.

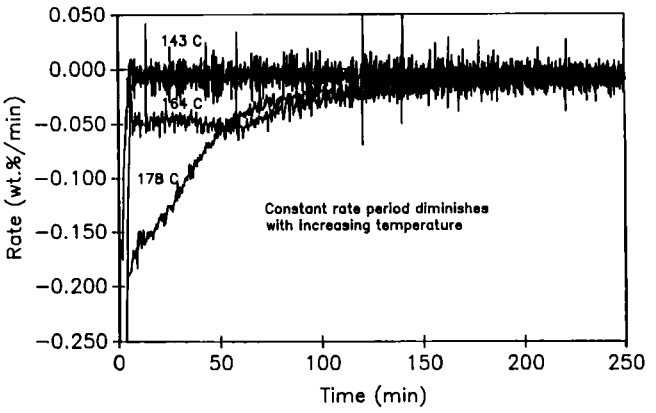

Fig. 11. Derivatives of data in Fig. 10.

Certainly, the results discussed above for the alumina–PVB–DBP composites are complicated by the presence of several organic components with greatly different volatilities. The eicosane composite, however, functions as a model system, albeit one with a lower viscosity. The TGA trace in Fig. 12 shows a rapid loss of eicosane at temperatures above 150°C, with a small loss between 200° and 400°C. This is similar to the vaporization of pure eicosane. Isothermal runs were performed at 120°C; Fig. 13 shows the constant-rate period measured when removing eicosane from the composite sheet. A representative mass flux derived from the constant rate period is 10^{-6} g/(s·cm^2). The tape adhered to the aluminum foil during each run and thus diffusion occurred through the top surface of the tape only.

The optical micrographs in Fig. 14 show the penetration of the potassium permanganate stain in progressively burned-out tapes. As seen in the alumina–PVB–DBP composite system, the stained region appeared to move as a front into the tape. In this case, however, evaporation occurred from the top surface only, so the stain moved from the top surface to the bottom. The stain can be observed thoughout the alumina–eicosane tape when as little as 40% of the eicosane was removed. These results support the conclusion reached previously: the simple diffusion model depicted in Fig. 1 cannot adequately describe the physical phenomena occurring during binder removal.

The fact that the PVB–DBP mixture has a viscosity many orders of magnitude larger than eicosane does not preclude the importance of capillary forces on the distribution of PVB–DBP during binder removal. Indeed, in a related study,[7] PVB–DBP mixtures were observed to move in tapered glass capillaries at 160°C. This motion was seen to occur in real time and always toward the narrow end of the capillary which, of course, has the largest suction pressure.

IV. Scaling Model for Capillary Forces During Thermolysis

The driving force for capillary flow must exceed the viscous resistance to flow if constant-rate drying or constant-rate binder removal are to be observed. An estimate of the driving force can be obtained from how pore sizes vary with packing of particles. Haines[8] calculated the characteristic size of pores formed between the waists of spherical particles packed in regular arrays. The suction pressure of a pore based on these calculations can be related to the particle size, as follows:

$$P_s = \frac{2\phi\gamma}{d} \tag{2}$$

where d is the particle diameter and ϕ is a factor dependent on the packing arrangement of the particles. Close packing of equally sized spheres produces the smallest pores, with $\phi = 12.9$, whereas a simple cubic arrangement of spheres has larger pores, with $\phi = 4.8$. A representative lower limit for the hydrostatic pressure difference required for capillary flow is the difference between the suction pressure from regions of close packing and that from regions of cubic packing. Thus, from Eq. (2), the driving force is given by

$$\Delta P = \frac{2\Delta\phi\gamma}{d} \tag{3}$$

where $\Delta\phi = (12.9 - 4.8) \approx 8$. This represents a conservative

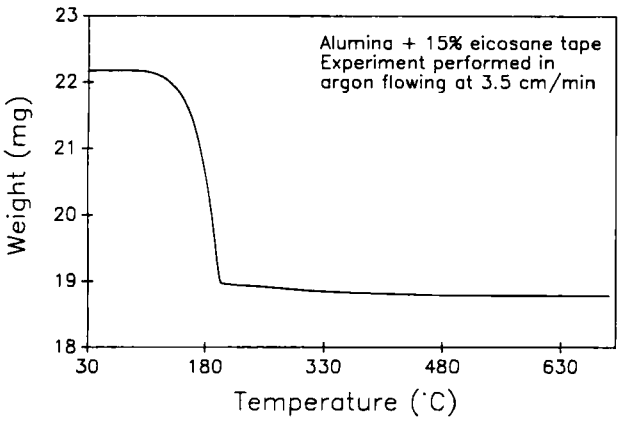

Fig. 12. Thermal gravimetric analysis of Al_2O_3–eicosane tape.

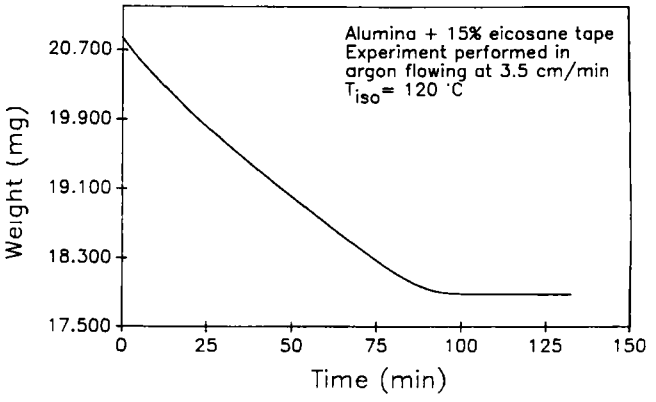

Fig. 13. Isothermal TGA indicating periods of constant rate of binder removal and falling rate of binder removal at T = 120°C.

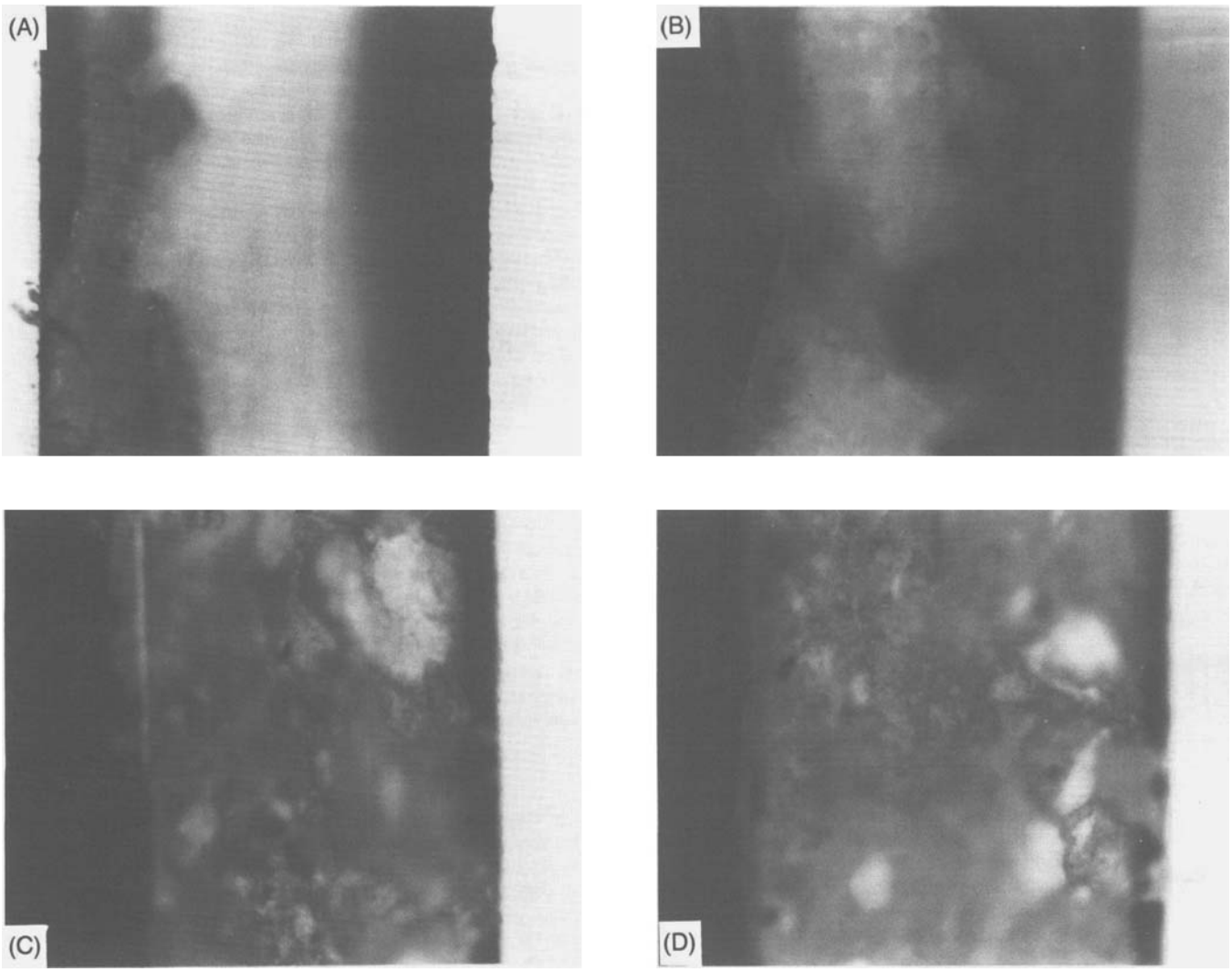

Fig. 14. Optical micrographs of the Al_2O_3–eicosane tape at various original weights of tape/binder burned out: (A) 97.0 wt%/20%, (B) 95.5 wt%/30%, (C) 94.0 wt%/40%, (D) 91.0 wt%/60%.

estimate of the capillary driving force since packing in the least-dense areas of the green body will certainly be less dense than cubic packing.

The hydrostatic driving force for flow described by Eq. (3) must be greater than the viscous pressure drop resulting from flow through porous media if a steady state is to be obtained. The magnitude of this pressure drop for a fully saturated porous media is given by the well-known Kozeny equation

$$\Delta P = \frac{36K\mu}{d^2}\frac{(1-\epsilon)^2}{\epsilon^3}hu \tag{4}$$

where μ is the viscosity of the fluid, ϵ is the void fraction of the porous body, and K is a constant that accounts for geometrical factors of the pores, such as their tortuosity and number of constrictions. Frequently, K is found to be on the order of 5 for most packed beds. The term u is the linear velocity of the fluid, and h is the distance over which flow occurs. If the porous body is not fully saturated, Eq. (4) must be modified to account for a decrease in the liquid conductivity.[9,10] For this discussion, Eq. (4) will be used to describe the lower limit on flow resistance. To judge the maximum-length scale over which capillary forces act, Eqs. (3) and (4) can be equated to give

$$\frac{h}{d} = \frac{\Delta\phi\epsilon^3}{18K(1-\epsilon)^2}\frac{\gamma}{\nu G} \tag{5}$$

where $\nu(=\mu/\rho)$ is the kinematic viscosity and $G(=\rho u)$ is the mass flux. The right side of Eq. (5) indicates, as expected, that the characteristic distance h, over which capillary flow is important, increases with increasing surface tension. This results from an increase in the driving force for flow. Correspondingly, h decreases as the viscosity and/or mass flux increases since the viscous losses become more important.

The right side of Eq. (5) divides naturally into two dimensionless quantities, one based on geometrical and packing parameters of the porous body and the other based on the physical characteristics of the liquid and the process. The tape considered in this study possessed a void fraction of 0.42, so Eq. (5) may be rewritten as

$$\log_{10} h/d = \log_{10}(\gamma/\nu G) - 1.7 \tag{6}$$

The data in Fig. 10 show that mass fluxes obtained between 143° and 164°C show constant-rate behavior. In this temperature range, the mass flux changed from 0.5×10^{-7} to 3.2×10^{-7} g/(cm^2 · s); the viscosity of the PVB–DBP mixture was 10^6 cP,[7] which, when combined with the values for G above and a representative surface tension of 10^{-5} N/cm (10 dyne/cm) for polymers, shows that the dimensionless group, $\log_{10}(\gamma/\nu G)$, changed from 4.2 at 143°C to 3.5 at 164°C. Equation (6) suggests that $\log_{10} h/d$ changes from 2.5 to 1.8 over this temperature range.

Scanning electron microscopy examination of the tape revealed

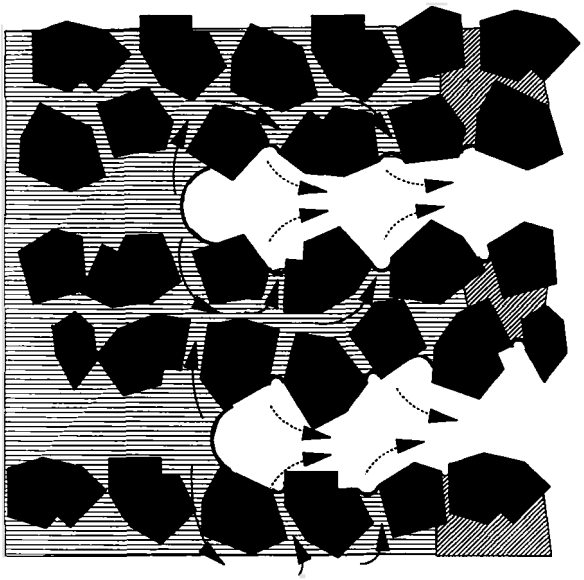

Fig. 15. Effect of capillary forces on a two-component binder. Deposition of nonvolatile component occurs in smallest pores (diagonally hatched).

a representative particle size of 0.3 μm. Thus, the characteristic distance over which capillarity was important changed from 95 to 20 μm when the temperature changed from 143° to 164°C. Since the half-thickness of the tape was 140 μm, the characteristic distance for capillarity changed from 70% to 15% of the dimensions of the tape as the temperature was raised. One would expect that the influence of capillarity on the binder distribution would diminish when h becomes much smaller than the dimensions of the body. The model supports the hypothesis that capillary forces significantly affect the distribution of this binder during thermolysis within the tape since the length scale over which capillarity is important is of the order of the dimensions of the tape.

V. Rejection of Nonvolatile Components

Evaporation of single-component solvents or binders from ceramic composites, as in the alumina–eicosane case described above, proceeds without the development of an internal mass-transfer resistance since capillarity draws liquid to the surface of the body. Multicomponent systems made of constituents with differing volatility undergo changes in binder composition as the binder is removed. Evaporation from the liquid–vapor interface in the multicomponent case produces a local enrichment of the nonvolatile component. If this species cannot diffuse at a high enough rate against the convective flux of the more volatile component, its local concentration continues to increase and, in the case of a polymer, may form a skin on the surface of the pore. This phenomenon is infrequently observed in the evaporation of solvents from particle films; a skin can form on the drying surface because of deposition of dispersants. Such a skin typically represents a significant mass-transfer resistance and the evaporation rate begins to fall.

One-dimensional diffusion in a two-component system from the situation described in Fig. 1, where the concentration of the volatile components is fixed to a low value at the liquid–vapor interface, has time-dependent solutions for the mass-transfer rate. The characteristic length for diffusion depends on time since volatile material must be drawn from deeper within the green body as it is removed. Thus, a steady-state solution for the mass-transfer rate does not exist in the case of a diffusion-controlling resistance in the condensed phase for a two-component system if diffusion is restricted to a single dimension.

A falling rate is not observed in the removal of DBP from DBP–PVB–alumina tapes at low removal rates. This seeming contradiction with behavior expected for two-component systems can be explained by liquid migration due to capillary forces. Constant-rate mass loss requires only that the controlling resistance to mass transfer remain constant throughout the drying process. For a single component, as discussed above, the constant controlling resistance is in the boundary layer external to the porous body. The characteristic length for diffusion remains constant in this boundary layer as long as the external conditions remain the same. A constant characteristic length for diffusion in the condensed phase can be envisioned by abandoning the simple one-dimensional model (Fig. 1) for the situation shown in Fig. 15. This figure depicts a highly idealized assembly of particles with a wide pore-size distribution. Initially, liquid is drawn to the smallest pores by capillary forces, but they become filled with the nonvolatile component. Small pores within the body continue to draw liquid from the large pores until they also become filled. The process is repeated and proceeds deeper into the green body. If the controlling mass-transfer resistance is in the vapor phase, then the characteristic length for diffusion increases with time and there is a decrease in the rate of removal of the volatile component. If, however, diffusion in the developing polymer film is controlling, then the diffusion distance remains constant and of the order of the length of the smallest pores. Diffusivities for the liquid- and gas-phase diffusion of DBP should differ by greater than 4 orders of magnitude; thus the distance over which diffusion takes place in the gas can be relatively large before it dominates the transport kinetics. The model proposed in Fig. 15 permits the establishment of steady-state behavior because capillarity opens pores to which volatile material can diffuse in a direction perpendicular to the pores; the model is thus not expected to behave as a one-dimensional diffusion problem.

VI. Conclusions

The distribution of binder within a green body during binder thermolysis plays an important role in the kinetics of the burnout process. Binder systems in which the binder melts have distributions that are dominated by capillary forces, depending on the physical properties of the molten binder and the rate at which volatile products are removed.

The development of penetrating porosity during the burnout process has several important implications. The characteristic lengths of diffusion for the situation described in Fig. 1 are very different from those when capillary-driven porosity develops throughout the body. Figure 1 describes a case where diffusion is controlled in the condensed phase because diffusion coefficients of volatile products in molten polymers are 4 orders of magnitude lower than that in the vapor phase, and because the characteristic lengths for the diffusion are of the same order of magnitude.

If one considers the case where porosity has developed throughout the body, however, the characteristic diffusion distance in the liquid is now half the distance between pores, and in its most developed state this distance will be the dimension of the particles. Thus, despite the difference in diffusivities, the controlling mass-transfer resistance may be in the vapor phase because of the difference in diffusion lengths. The reported higher yields of injection-molded parts when dewaxed under high ambient pressure[11] can in part be understood by a vapor-phase-controlling mechanism.

Enhancement of capillary forces during binder thermolysis may provide certain process advantages. The binder is removed homogeneously from the green body when capillary forces draw liquid to the surface; thus large gradients in stress are avoided. The simple model described above indicates which physical properties must be controlled to enlarge the scale over which capillary action is important. Two obvious parameters are surface tension and viscosity. Increasing the surface tension of the molten binders will increase the driving force for capillary flow, whereas decreasing the viscosity lowers the resistance to that flow. A viscosity that is too low, of course, will create difficulties due to the possibilty of deformation or slumping during thermolysis. Many of the successful binder systems used in practice are composed of many components with differing volatilities. These components provide a variety of functions, and may also act to enhance capil-

larity by lowering the viscosity.

Capillary forces have been shown to greatly influence the distribution of binder in a case where the viscous and surface-tension properties of the system are such that, during thermolysis, binder can move at a rate comparable to the mass flux of volatile products.

Binder systems that do not melt, such as thermosetting resins, will not be subject to capillary forces. The development of porosity during thermolysis in these systems may also differ from that simplistically illustrated in Fig. 1. Current research is now focusing on binder systems that do not melt, in an effort to model the relationship between the characteristics of the binder and its distribution for these systems.

Acknowledgments: The authors are indebted to Dr. W. Rhine and Prof. P. Calvert for their advice.

References

[1]R. E. Mistler, D. J. Shanefield, and R. B. Runk, "Tape Casting of Ceramics"; pp. 411–48 in Ceramic Processing Before Firing. Edited by G. Y. Onoda and L. L. Hench. Wiley, New York, 1978.

[2]G. C. Wall and R. J. C. Brown, "The Determination of Pore-Size Distribution from Sorption Isotherms and Mercury Penetration in Interconnected Pores: The Application of Percolation Theory," *J. Colloid Interface Sci.*, **82** [1] 141–49 (1981).

[3]J. F. Pearse, T. R. Oliver, and D. M. Newitt, "The Mechanism of the Drying of Solids," *Trans. Inst. Chem. Eng.*, **27**, 1 (1949).

[4]E. W. Comings and T. K. Sherwood, "The Drying of Solids," *Ind. Eng. Chem.*, **26**, 1096–98 (1934).

[5]N. H. Ceaglske and O. A. Hougen, "The Drying of Granular Solids," *Trans. Am. Inst. Chem. Eng.*, **33**, 283–314 (1937).

[6]T. M. Shaw, "Liquid Redistribution During Liquid-Phase Sintering," *J. Am. Ceram. Soc.*, **69** [1] 27–34 (1986).

[7]M. J. Cima, M. Dudziak, and T. A. Lewis, "Observation of PVB–DBP Binder Capillary Migration," *J. Am. Ceram. Soc.*, **72** [6] 1087–90 (1989).

[8]W. B. Haines, "Studies in the Physical Properties of Soils, IV. A Further Contribution to the Therory of Capillary Phenomena in Soil," *J. Agr. Sci.*, **17**, 264 (1927).

[9]R. E. Collins, Flow of Fluids Through Porous Materials; p. 54. Reinhold, New York, 1961.

[10]T. M. Geffen, W. W. Owens, D. R. Parrish, and R. A. Morse, "Experimental Investigation of Factors Affecting Laboratory Relative Permeability Measurements," *Petroleum Trans., AIME*, **192**, 99–110 (1951).

[11]B. C. Mutsuddy, "A Review of Binder Removal Processes for Ceramic Injection Molded Parts," AIChE Conference on Emerging Technologies in Materials, Minneapolis, MN, Aug. 18–20, 1987. □

journal

J. Am. Ceram. Soc., **72** [7] 1199–207 (1989)

Defect Structure of Cobalt Monoxide: I, The Ideal Defect Model

Janusz Nowotny and Mieczyslaw Rekas*

Max-Planck-Institute for Solid-State Research, 7000 Stuttgart 80, Federal Republic of Germany

The nonstoichiometry and electrical properties of $Co_{1-y}O$ are considered in terms of an ideal defect model. Both intrinsic and extrinsic regions are analyzed. Interrelationships between the oxygen partial pressure and the oxide composition are derived. It has been shown that the p_{O_2} exponent resulting from the deviation from stoichiometry ($1/n_y$) differs substantially from the exponent determined by measurements of electrical conductivity ($1/n_\sigma$). The limitations of the ideal defect approximation are discussed. [Key words: cobalt oxide, defects, modeling, nonstoichiometry.]

I. Introduction

THE transition-metal monoxides such as NiO, CoO, and FeO have been receiving considerable attention as model materials for elucidation of defect structures and the nature of interactions between the defects. These oxides are known to be metal deficient and can be generally expressed by the formula $M_{1-y}O$. Specific properties of these materials are closely related to their nonstoichiometry. The extent of the deviation from stoichiometric composition (y) increases from about 0.001 for NiO to 0.01 for CoO and as high as 0.16 for FeO. It is generally agreed that at low concentrations of defects (case of NiO) the defect structure can be well explained by an ideal defect model. On the other hand, higher concentrations of defects result in strong interactions leading to the formation of complex defect assemblies, aggregates, or clusters, as reported for FeO. CoO exhibits intermediate defect properties between those of NiO and FeO.

The stability range of the CoO phase field is illustrated in Fig. 1 for T vs $\log p_{O_2}$ with various values of the nonstoichiometry y.[1,2] As can be seen, y varies between 0.0001 at low p_{O_2} and 0.012 at the CoO/Co_3O_4 phase boundary.

It has been reported that the nonstoichiometry in CoO results in cation vacancies and electron holes. Recent studies have shown that cobalt interstitials also may be formed.[3] These defects, however, may be stable only in the outer surface layer at high nonstoichiometry in the vicinity of the CoO/Co_3O_4 phase boundary.[3]

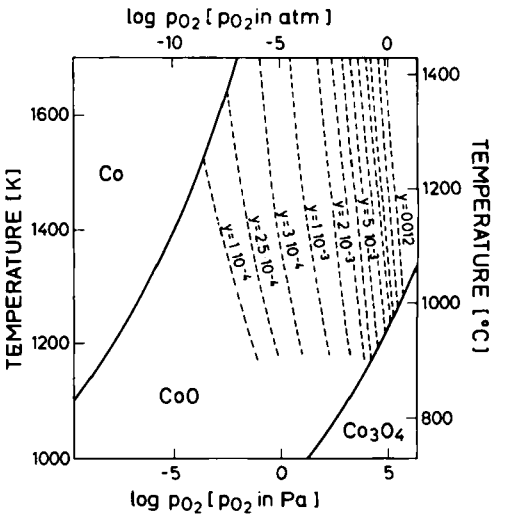

Fig. 1. Stability range of $Co_{1-y}O$.[1,2]

K. E. Spear—contributing editor

Manuscript No. 199130. Received May 19, 1988; approved November 22, 1988.
The authors dedicate this paper to Professor Adam Bielański on the occasion of his 75th birthday.

*On leave from the Institute of Materials Science, Academy of Mining and Metallurgy, 30059 Krakow, Poland.